Cellulose nanocrystals/zeolitic imidazolate framework-L(CNCs/ZIF-L) composites for loading and diffusion-controlled release of doxorubicin hydrochloride

by Christian J. Wijaya

Journal of the Taiwan Institute of Chemical Engineers 165 (2024) 105831

Contents lists available at ScienceDirect

Journal of the Taiwan Institute of Chemical Engineers

journal homepage: www.journals.elsevier.com/journal-of-the-taiwan-institute-of-chemical-engineers

Cellulose nanocrystals/zeolitic imidazolate framework-L (CNCs/ZIF-L) composites for loading and diffusion-controlled release of doxorubicin hydrochloride

Christian J. Wijaya [a,b,*], Sandy B. Hartono [a,b], Jindrayani N. Putro [a,b], Juliana Anggono [b,c], Tarzan Sembiring [b,d], Herlian E. Putra [b,d], Maria Yuliana [a,b], Jenni Lie [a,b], Shella P. Santoso [a,b], Chien-Yen Chen [e,f], Felycia E. Soetaredjo [a,b], Suryadi Ismadji [a,b], Setiyo Gunawan [g]

[a] Department of Chemical Engineering, Widya Mandala Surabaya Catholic University, Kalijudan 37, Surabaya 60114, Indonesia
[b] Collaborative Research Center for Zero Waste and Sustainability, Widya Mandala Surabaya Catholic University, Kalijudan 37, Surabaya 60114, Indonesia
[c] Department of Mechanical Engineering, Petra Christian University, Siwalankerto 121-131, Surabaya, 60236, Indonesia
[d] Research Center for Environmental and Clean Technology, National Research and Innovation Agency, Republic of Indonesia, KST Samaun Samadikun, Bandung, 40135, Indonesia
[e] Department of Earth and Environmental Sciences, National Chung Cheng University, 168 University Road, Min-Hsiung, Chiayi County 62102, Taiwan
[f] Center for Nano Bio-Detection, Center for Innovative Research on Aging Society, AIM-HI, National Chung Cheng University, 168, University Road, Min-Hsiung, Chiayi County 62102, Taiwan
[g] Department of Chemical Engineering, Faculty of Industrial Technology and Systems Engineering, Institut Teknologi Sepuluh Nopember, Keputih Sukolilo, Surabaya 60111, Indonesia

ARTICLE INFO

Keywords:
Cellulose nanocrystals
Composite
Doxorubicin hydrochloride
Drug carrier
Zeolitic imidazolate framework-L

ABSTRACT

Background: Zeolitic imidazolate framework-L (ZIF-L) has great potential as a doxorubicin hydrochloride (DOX) drug carrier for oral chemotherapy applications. This medical application will greatly support the development of cancer treatment and reduce the cancer fatality rate. However, ZIF-L as a type of metal-organic framework (MOFs) faces several challenges to be implemented in biomedical applications which impact the drug loading and release mechanisms.

Methods: CNCs/ZIF-L composites were fabricated via a green in-situ method using CNCs mass percentages of 2.5, 5, 7.5, and 10 % of $Zn(NO_3)_2{\cdot}6H_2O$. All composites were tested for the DOX loading and release mechanisms and antioxidant activity.

Significant findings: Here, the addition of CNCs enhances the DOX loading capacity of CNCs/ZIF-L composite up to 1508.91 ± 7.72 mg/g due to the presence of abundant active functional groups. In addition, the DOX release profile is another interesting potential that occurs through a diffusion-controlled release mechanism. This shows the ability of CNCs/ZIF-L composite to deliver drugs orally where DOX is released consistently at a certain concentration level for prolonged treatment. Moreover, the IC_{50} value of DOX@CNCs/ZIF-L drug reaching 480.21 mg/L proves that the effectiveness of DOX is maintained even though it is administered orally in the form of solid material.

1. Introduction

Cancer is a disease that is quite deadly so far, which can attack and spread to various organs of the body with varying levels of malignancy. In 2020, there were around 19 million new cancer cases worldwide dominated by breast, lung, prostate, colon, and stomach cancer. Moreover, what needs to be worried about is the mortality rate which reached 140.7 per 100,000 for men and 114.6 per 100,000 for women. In Indonesia itself, around 400,000 cases in 2020 were detected with 16.9 % of them being breast cancer. The best and most common treatment that can be given to cancer sufferers is chemotherapy, where chemotherapy drugs can inhibit or stop the growth of cancer cells. However, intravenous (IV) chemotherapy treatment, which has been widely used up to now, can also have negative impacts on healthy human cells,

* Corresponding author.
E-mail address: christian_wijaya@ukwms.ac.id (C.J. Wijaya).

https://doi.org/10.1016/j.jtice.2024.105831
Received 14 May 2024; Received in revised form 30 September 2024; Accepted 11 November 2024
Available online 15 November 2024

tissues, nerves, and organs because chemotherapy drugs have a high destructive level [1]. This can be indicated by the side effects that appear after chemotherapy treatment where sufferers experience nausea, vomiting, decreased blood components, hair loss, and blackened nails [2]. Therefore, chemotherapy treatment continues to be developed to reduce these side effects, one of which is oral chemotherapy where chemotherapy drugs are delivered by a drug carrier through the human digestive system. In this case, advanced materials that are safe and have the potential to act as drug carriers need to be developed to avoid the side effects of chemotherapy drugs while facilitating the ability to target more specific cancer locations.

Metal-organic frameworks (MOFs) are one of the advanced materials that are being widely investigated for several applications, such as drug delivery systems [3–5] and wastewater treatments [6–8]. MOFs are 2D or 3D materials with a large surface area, good thermal stability, adaptable structure, and a variety of functions [9–11]. In addition, MOFs are easy to functionalize with other materials to improve their characteristics and meet the needs of specific applications [12]. However, the application of MOFs has its challenges, such as (1) the tendency to have low conductivity (10^{-10} – 10^{-7} S/m for ZIFs) or neutral charge [13,14], (2) the tendency to have difficulty maintaining its macroscopic shape and hierarchical porosity (macro-to-micro or micro-to-meso pores) [11, 15], (3) the tendency to easily agglomerate, (4) low stability in water, and (5) difficult to reuse [10,16]. In this medical application, the functionalization of MOFs is necessary to overcome these challenges. In previous studies, several functionalization materials showed great potential in drug delivery applications, such as cellulose-based materials [17], chitosan-based materials [18], and metal oxides [19]. This study combined both materials, namely MOFs and cellulose-based materials, into a composite material which is expected to enhance its ability as a drug carrier. As one of the cellulose-based materials, cellulose nanocrystals (CNCs) are porous crystalline materials that are biodegradable, biocompatible, non-toxic, charged, and cannot be digested by humans so they can be applied in composite materials for drug carriers [20,21]. CNCs are suitable as a functionalization material of MOFs due to the abundant availability of cellulose, the smaller size of CNCs than MOFs, and the excellent properties of CNCs. Here, the presence of CNCs is expected to provide additional negative charges impacting the potential interaction with drug molecules and the loading capacity. This negative charge can also have an impact on material agglomeration and stability in solvents.

In this study, zeolitic imidazolate framework-L (ZIF-L), one type of MOFs, was combined with CNCs to form CNCs/ZIF-L composites. The fabrication of CNCs/ZIF-L composites was proposed using a water-based solvent at room temperature so that it is more environmentally friendly and energy efficient. Here, the addition of CNCs was studied to obtain the best CNCs/ZIF-L composite for the loading and release of doxorubicin hydrochloride (DOX). Moreover, the kinetics and isotherm studies were performed to understand the loading and release mechanism of DOX onto/from CNCs/ZIF-L composite. This composite material was expected to be a good drug carrier for DOX without reducing the treatment effectiveness of DOX itself.

2. Experimental

2.1. Materials

Zinc nitrate hexahydrate ($Zn(NO_3)_2{\cdot}6H_2O$, 98 %), 2-methylimidazole (Hmim, 99 %), ethanol (C_2H_5OH, 99.9 %), sulfuric acid (H_2SO_4, 96 %), doxorubicin hydrochloride (DOX, 100 %), Whatman filter paper (Grade 40), 2,2-diphenyl-1-picrylhydrazyl (DPPH, 100 %), methanol (CH_3OH, 99.8 %), and ascorbic acid ($C_6H_8O_6$, 99 %) were purchased from Sigma-Aldrich (Singapore) as an analytical grade and used without further treatment.

2.2. Preparation of CNCs

Whatman filter paper was used as the cellulose source for isolating CNCs based on the method that has been developed from previous studies [22–24]. Shredded filter paper (5 g) was hydrolyzed using 100 mL of sulfuric acid solution (55 wt%) at 40 °C for one hour under continuous stirring. After the hydrolysis process was complete, 10-fold cold distilled water was added to stop the process. The solids were then separated from the supernatant using a centrifuge (9500 × *g*) for 10 min. After that, the turbid supernatant was dialyzed with distilled water using a dialysis membrane tube (Spectrum™ Spectra/PorTM, 12–14 kDa of MWCO) until the pH was neutral. Then, the suspension was sonicated for 20 min before being frozen for the freeze-drying process. Finally, dried CNCs were obtained using a freeze dryer at 0.08 mbar and –42 °C.

2.3. Fabrication of ZIF-L and CNCs/ZIF-L composites

The optimum condition for ZIF-L fabrication has been reported in a previous study which was also used here for ZIF-L fabrication and then developed for the fabrication of CNCs/ZIF-L composites [1]. In the fabrication of ZIF-L, two solutions were prepared separately in 40 mL of distilled water, Solution A containing $Zn(NO_3)_2{\cdot}6H_2O$ (0.075 M) and Solution B containing Hmim (0.617 M). Both solutions were sonicated for 10 min to homogenize the solutions and then Solution A was added slowly to Solution B under continuous stirring. This process was maintained at 29 °C for 97 min while the ZIF-L solids formed and made the suspension cloudy. Further, ZIF-L was separated using a centrifuge for 10 min and washed with two times distilled water and two times ethanol. Finally, ZIF-L was dried using an oven at 80 °C.

CNCs/ZIF-L composites were fabricated using the same procedure as ZIF-L with the in-situ addition of CNCs. Here, CNCs were added to Solution A before the two solutions were mixed. The effects of adding CNCs were investigated by varying the mass of CNCs by 2.5, 5, 7.5, and 10 % of $Zn(NO_3)_2{\cdot}6H_2O$. Here, the composites obtained were coded as CNCs/ZIF-L(2.5), CNCs/ZIF-L(5), CNCs/ZIF-L(7.5), and CNCs/ZIF-L(10), respectively. Further, all composites were characterized and tested for best loading capacity towards DOX where batch adsorption was performed for each composite using aqueous DOX solution.

2.4. Characterizations

In this study, ZIF-L and CNCs/ZIF-L composites were characterized using several instrumentations to investigate their physical and chemical characteristics. Scanning electron microscopy (SEM) analysis was carried out to depict the morphology of samples using a JEOL JSM-6500F field emission SEM. This analysis was conducted in conjunction with an energy-dispersive X-ray (EDX) analysis to map the elemental distribution of samples. In this analysis, the samples were coated with conductive platinum using JEOL JFC-1200 coated in an argon atmosphere. X-ray diffraction (XRD) analysis was performed to investigate the diffractogram and its crystallinity of samples using a Philips PANalytical X'Pert Pro X-ray diffractometer. It was done with Cu $K\alpha_1$ (λ = 1.54 Å) as the radiation source at a voltage of 40 kV, a current of 30 mA, and a step size of 0.02°/step. Fourier transform infrared spectroscopy (FTIR) analysis was conducted to investigate the functional groups of samples using a Shimadzu 8400S FTIR with the KBr pelleting method (4000–400 cm^{-1}).

2.5. Loading of DOX on CNCs/ZIF-L composite

All DOX loading experiments were carried out using the batch adsorption method with 10 mL of aqueous DOX solution (160.50 mg/L) for each batch. In the kinetics study, 10,000 μg of CNCs/ZIF-L composite was added to the aqueous DOX solution and administered in a shaking water bath at room temperature for a time range of 10 min to 24 h. Meanwhile, the isotherm study was performed using a mass range of

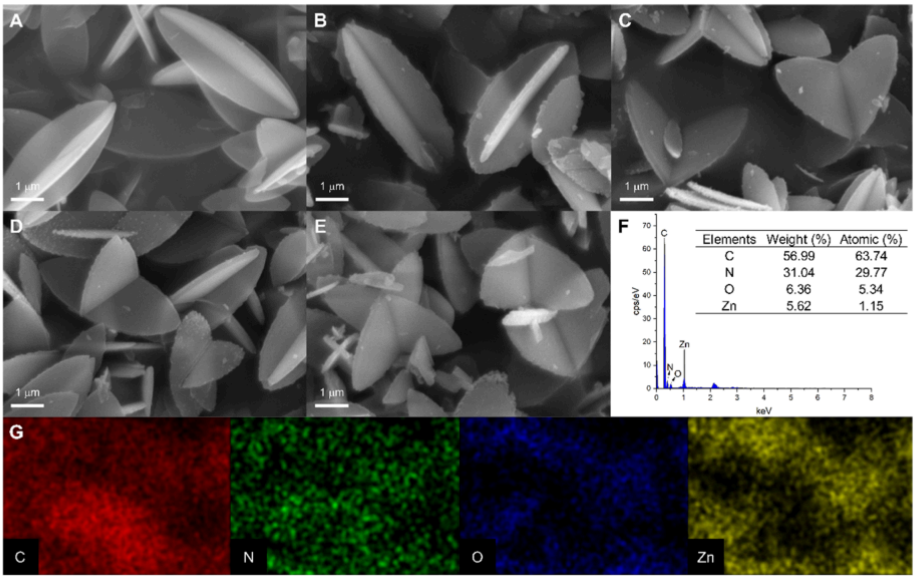

Fig. 1. Morphologies of (A) ZIF-L, (B) CNCs/ZIF-L(2.5), (C) CNCs/ZIF-L(5), (D) CNCs/ZIF-L(7.5), and (E) CNCs/ZIF-L(10) composites based on SEM analysis including (F) EDX analysis and (G) EDX mapping for CNCs/ZIF-L(5) composite.

CNCs/ZIF-L composite of 500 to 20,000 μg at room temperature for an equilibrium time obtained from the kinetic study. Here, the concentration of the remaining DOX solution was measured using a Shimadzu UV/Vis Spectrophotometer 2600 at a wavelength of 475 nm. Further, loading capacities for kinetic and isotherm studies were expressed as q_t (mg/g) and q_e (mg/g), respectively, and calculated by these equations [26]:

$$q_t = \frac{(C_i - C_f)V}{m} \quad (1)$$

$$q_e = \frac{(C_i - C_e)V}{m} \quad (2)$$

where C_i,C_f and C_e express the initial DOX concentration, the remaining DOX concentration at a certain time, and the equilibrium DOX concentration, respectively, while V and m are the volume of solution and the mass of CNCs/ZIF-L composite used in the loading system. Further, the DOX loading data were modelled using several kinetic and isotherm adsorption models.

2.6. Release of DOX from DOX@CNCs/ZIF-L drug

The release study was performed through a dialysis membrane method using DOX@CNCs/ZIF-L drug obtained from the loading experiment. In this study, 250 mg of DOX@CNCs/ZIF-L drug was mixed into 10 mL of PBS solution with a pH of 7.4. Next, the mixture was put in a dialysis membrane tube (Spectrum™ Spectra/PorTM, 12–14 kDa of MWCO) and immersed into 500 mL of PBS solution at 37 °C. At each certain time, 3 mL of PBS solution containing DOX released from the DOX@CNCs/ZIF-L drug was sampled for 10 min to 72 h and replaced with 3 mL of fresh PBS solution to keep the total volume of the drug release system constant. Here, the concentration of samples was measured using a Shimadzu UV/Vis Spectrophotometer 2600 at a wavelength of 475 nm. Further, the release profile was expressed in terms of cumulative release percentage.

2.7. Antioxidant activity analysis

As a preliminary test of drug effectiveness, antioxidant activity analysis was carried out using the DPPH assay for free DOX, CNCs/ZIF-L composite, and DOX@CNCs/ZIF-L drug to investigate the free radical inhibition ability of the samples. Initially, the DPPH solution was prepared by dissolving 4 mg of DPPH into 100 mL of methanol. Next, 1 mL of sample at a certain concentration was mixed with 3 mL of DPPH solution in a test tube and incubated at room temperature for 30 min in the dark room. After that, the absorbance was measured using a Shimadzu UV/Vis Spectrophotometer 2600 at a wavelength of 517 nm. Here, the DPPH radical scavenging (%) was calculated by the following equation [27,28]:

$$DPPG\ radical\ scavenging = \frac{Abs_{blank} - Abs_{sample}}{Abs_{blank}} \times 100\% \quad (3)$$

where Abs_{sample} and Abs_{blank} are the absorbances of the DPPH solution after exposure to the sample and without the sample (or solvent only). In this analysis, ascorbic acid was used as a positive control which can effectively inhibit free radicals. In addition, the parameter IC_{50} could be determined when the DPPH radical scavenging reached 50 % and was expressed in sample concentration.

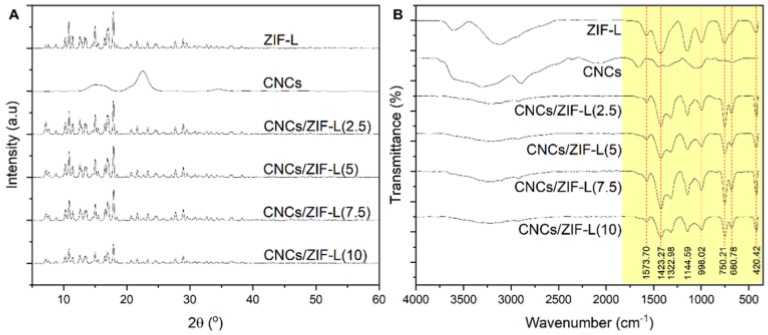

Fig. 2. (A) XRD diffractograms and (B) FTIR spectra of ZIF-L, CNCs, and CNCs/ZIF-L composites.

3. Results and discussion

3.1. Characterizations of CNCs/ZIF-L composites

Here, CNCs/ZIF-L composites have been successfully fabricated using the in-situ method at room temperature. Fig. 1 shows the morphologies of fabricated materials captured by SEM analysis. The basic framework of these composites is the same as their main precursor (ZIF-L) which has a starfruit-like morphology as reported in the previous study (Fig. 1A) [25]. As reported in the previous study, the size of CNCs is about 145 nm which so much lower than the size of ZIF-L (± 5 μm) fabricated in this study [22]. Therefore, the presence of CNCs in these composites is located on the surface of ZIF-L as shown in Fig. 1 (B, C, D, E) so it makes the surface rougher compared to ZIF-L. In addition, the higher CNC composition added to the fabrication system causes the composite surface to become rougher, especially at the morphological edges. Fig. 1 (F, G) shows the EDX analysis and mapping indicating higher carbon and oxygen contents up to 56.99 and 6.36 wt% for CNCs/ZIF-L(5) composite, respectively. The carbon and oxygen contents in these composites are increased compared to ZIF-L itself (53.52 wt% of carbon and 5.49 wt% of oxygen) as reported in previous studies due to the presence of CNCs in the composites [25].

From the composite morphology, ZIF-L is more dominant in terms of composite structure compared to CNCs due to their particle size. These results are also in agreement with the XRD diffractograms and FTIR spectra obtained. CNCs/ZIF-L composites have lattice planes and functional groups come from their precursors (ZIF-L and CNCs). As presented in Fig. 2(A), the XRD diffractograms of CNCs/ZIF-L composites show lattice planes very similar to those of ZIF-L, such as (110), (200), (211), (220), (310), and (222), which seen at 2θ of 7.65°, 10.28°, 12.62°, 15.02°, 16.56°, and 17.91° for CNCs/ZIF-L(5) composite, respectively. In the FTIR spectra (Fig. 2B), the CNCs/ZIF-L composites have the same functional groups combined by ZIF-L and CNCs that are specifically indicated in the fingerprint area of these spectra. Here, Zn–N stretching (420.42 cm^{-1}), out-of-plane bending of aromatic rings (680.78 and 750.21 cm^{-1}), C–N stretching (998.02 cm^{-1}), C=N stretching (1144.59 cm^{-1}), aromatic ring stretching (1423.27 cm^{-1}), and N–H stretching (1573.70 cm^{-1}) represent the functional groups of ZIF-L in the CNCs/ZIF-L composites [25,29–33]. Meanwhile, the CH_2 rocking of the glucose cyclic chain presented at 1322.98 cm^{-1} in the composite spectra reflects the CNCs content [23,34]. Based on the characterizations, all composites provide similar appropriate characteristics so that the best composite can be determined further by their loading capacity towards DOX.

Preliminary DOX loading experiments have been conducted to investigate the best percentage of CNCs added to the in-site composite fabrication. These experiments are carried out via batch adsorption with very excessive time (24 h) to reach the equilibrium stage. Fig. 3 shows a comparison of the loading capacities of ZIF-L, CNCs, and CNCs/ZIF-L composites where the single materials (ZIF-L and CNCs) have loading capacities on DOX reaching 961.30 ± 19.70 and 479.91 ± 15.94 mg/g, respectively. Even though CNCs have a lower loading capacity than ZIF-L, CNCs have been proven to enhance the loading capacity of the CNCs/ZIF-L composites due to their abundant surface functional groups. These functional groups can interact with DOX having rich hydroxyl, carbonyl, and amine groups to create higher molecular interactions and loading capacity. Here, the CNCs/ZIF-L(5) composite has the highest DOX loading capacity of up to 1508.91 ± 7.72 mg/g with an increase of 56.96 % from the loading capacity of single ZIF-L and 214,42 % from the loading capacity of single CNCs. Therefore, the addition of CNCs at 5 % of the metal precursor had the best impact on increasing the DOX loading capacity. In comparison to a previous study, the CNCs/ZIF-L(5) provides a higher DOX loading capacity compared to silica-modified magnetic iron oxide which has 58,1 % of drug loading efficiency or approximately 69,72 mg/g of loading capacity [35].

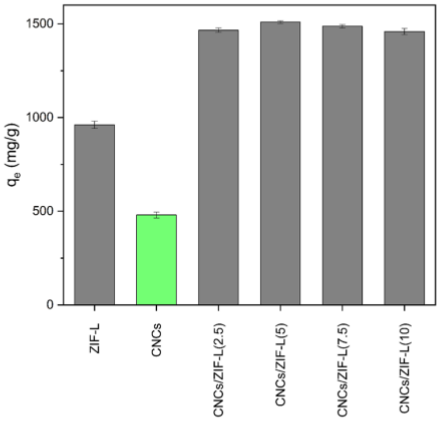

Fig. 3. Loading capacities of ZIF-L, CNCs, and CNCs/ZIF-L composites towards DOX.

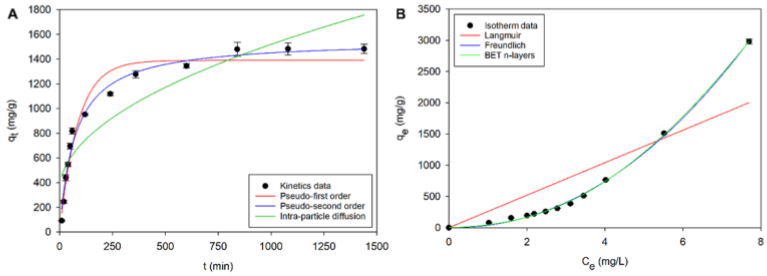

Fig. 4. (A) Kinetics and (B) isotherm modelling of DOX loading on CNCs/ZIF-L composite.

Table 1
Kinetics and isotherm modelling parameters of DOX loading on CNCs/ZIF-L composite.

Models	Parameters	Values
Kinetics models		
Pseudo-first order, $q_t = q_e(1 - e^{-k_1 t})$	q_e – equilibrium loading capacity (mg/g)	1389.54
	k_1 – time scaling factor (1/min)	0.0116
	R^2	0.9706
Pseudo-second order, $q_t = q_e\left(\frac{q_e k_2 t}{1 + q_e k_2 t}\right)$	q_e – equilibrium loading capacity (mg/g)	1557.01
	k_2 – time scaling factor (g/mg.min)	8.73×10^{-6}
	R^2	0.9875
Intra-particle diffusion, $q_t = k_d\sqrt{t} + C$	k_{d1} – rate constant for early-stage (mg/g.min$^{0.5}$)	87.66
	k_{d2} – rate constant for mid-stage (mg/g.min$^{0.5}$)	29.78
	k_{d3} – rate constant for end-stage (mg/g.min$^{0.5}$)	9.27
	k_d – rate constant for overall stage (mg/g.min$^{0.5}$)	40.07
	C – intercept (mg/g)	271.48
	R^2	0.8425
Isotherm models		
Langmuir, $q_e = \frac{q_{max} K_L C_e}{1 + K_L C_e}$	q_{max} – maximum loading capacity (mg/g)	8.24×10^7
	K_L – Langmuir constant (L/mg)	3.16×10^{-6}
	R^2	0.7441
Freundlich, $q_e = K_F C_e^{1/n_F}$	K_F – Freundlich constant ((mg/g)(mg/L)$^{-n}$)	38.60
	n_F – heterogeneity (–)	0.4692
	R^2	0.9986
BET n-layers, $q_e = \frac{q_{max} K_{BF} C_e \left[1 - (n_B + 1)(K_{BU} C_e)^{n_B} + n_B (K_{BU} C_e)^{n_B + 1}\right]}{(1 - K_{BU} C_e)\left[1 + \left(\frac{K_{BF}}{K_{BU}} - 1\right) K_{BU} C_e - \left(\frac{K_{BF}}{K_{BU}}\right)(K_{BU} C_e)^{n_B + 1}\right]}$	q_{max} – maximum loading capacity on the first layer (mg/g)	297.30
	K_{BF} – first-layer equilibrium constant (L/mg)	0.0031
	K_{BU} – upper-layer equilibrium constant (L/mg)	0.4661
	n_B – number of layers	337.77
	R^2	0.9990

3.2. Kinetic and isotherm studies of DOX loading on CNCs/ZIF-L composite

DOX loading has been investigated through adsorption kinetics and isotherm using CNCs/ZIF-L(5) composite as the best composite in this study. Fig. 4(A) shows the kinetic profile of DOX loading on CNCs/ZIF-L (5) composite and its non-linear modelling using pseudo-first order, pseudo-second order, and intra-particle diffusion equations. Here, pseudo-second order is more well-fitted to the data ($R^2 = 0.9875$) compared to pseudo-first order ($R^2 = 0.9706$) and intra-particle diffusion ($R^2 = 0.8425$). It means that the loading mechanism occurs by chemisorption where the interactions between CNCs/ZIF-L(5) composite and DOX are built by chemical bonding. This supports the hypothesis above that the loading capacity is strengthened by the chemical interactions between the functional groups of CNCs/ZIF-L(5) composite and DOX. However, it does not rule out the possibility that physisorption also occurs in this loading mechanism because the compatibility to the pseudo-first order is also quite good ($R^2 > 0.95$). Table 1 presents the values of each modeling parameter obtained here where q_e and k_2 of pseudo-second order exhibit the equilibrium loading capacity and how fast the equilibrium stage can be reached. In terms of q_e, the value of 1557.01 mg/g is in line with the results of preliminary experiments which proves that the equilibrium stage has been reached within 12 h. In addition, the k_2 value is dependent on initial concentration and time which is strongly correlated with the loading rate [36]. In Table 1, the k_2 of 8.73×10^{-6} g/mg.min can be categorized as a small value indicating a low loading rate. This underlies the fact that a fairly long equilibrium time of up to 12 h is found.

Another modelling with intra-particle diffusion provides an interpretation of the loading mechanism in three stages according to the kinetic profile obtained, such as (1) DOX diffusion through the bulk solution towards the interface, (2) DOX diffusion through the interface, and (3) formation of bonding interactions between CNCs/ZIF-L(5) composite and DOX through their functional groups. In Table 1, the values of k_{d1},k_{d2} and k_{d3} indicate those three stages of DOX loading on CNCs/ZIF-L composite. Here, k_{d1} gives the highest value (87.66 mg/g.min$^{0.5}$) compared with the other two parameters indicating that DOX diffusion through the bulk solution has greater resistance and plays a bigger role in the loading mechanism.

Further, an isotherm study has been conducted and presented in Fig. 4(B) including the non-linear modelling using Langmuir, Freundlich, and BET n-layers equations. Here, the isotherm profile is well-fitted with Freundlich and BET n-layers equations which are represented by the R^2 values of 0.9986 and 0.9990, respectively. In terms of Freundlich

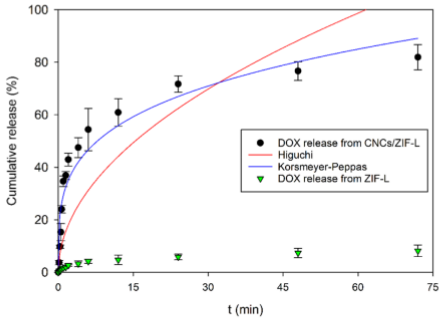

Fig. 5. DOX cumulative release from DOX@CNCs/ZIF-L drug with its kinetics modelling and from DOX@ZIF-L drug.

parameters, n_F indicates the heterogeneous active sites of CNCs/ZIF-L(5) composite because its value is less than unity [37]. Lower n_F value or greater heterogeneity provides higher energy difference and capability in the loading mechanism. Moreover, the DOX loading on CNCs/ZIF-L (5) composite here occurs through a multilayer mechanism based on its fitness with the BET *n*-layers equation. The q_{max} represents the loading capacity of the first DOX layer on CNCs/ZIF-L(5) composite reaching up to 297.30 mg/g or about 19.7 % of overall loading capacity. However, the ratio between the first- and upper-layer equilibrium constants (K_{BF}/K_{BU}) is very small exhibiting higher loading capacity on the upper layer. This phenomenon promotes a larger number of DOX layers presented on the CNCs/ZIF-L composite corresponding to the great n_B value. Furthermore, the isotherm profile in Fig. 4(B) is classified as Type III Isotherm based on the IUPAC classification [38]. This type exhibits that CNCs/ZIF-L(5) composite is categorized as a non-porous material and the loading mechanism occurs in a multilayer system [39]. In this case, a previous study has reported that ZIF-L as the main precursor in this CNCs/ZIF-L(5) composite is a non-porous material [40].

3.3. DOX release study from DOX@CNCs/ZIF-L drug

Fig. 5 shows the DOX release profile from DOX@CNCs/ZIF-L drug and its modelling using Higuchi and Korsmeyer-Peppas equations. This cumulative release profile refers to the diffusion-controlled release mechanism of DOX from DOX@CNCs/ZIF-L drug. The diffusion-controlled release mechanism shows that DOX is released up to a certain cumulative percentage at the early stage and then remains fairly constant at a certain value [41]. This mechanism categorizes the CNCs/ZIF-L(5) composite as a drug reservoir that can prolong or instantly release DOX depending on the characteristics of the composite material. In the modelling study, the Korsmeyer-Peppas equation is more fitted compared to the Higuchi equation which means that the DOX release from DOX@CNCs/ZIF-L drug involves three main processes, such as water diffusion into the drug framework, swelling of the drug framework, and dissolution of the drug framework [42]. The presence of CNCs in the composite structure enhances the loading capacity but also triggers the swelling and dissolution of the composite. This is proven by a significant increase in DOX release percentage when compared to using ZIF-L alone as shown in Fig. 5. The DOX release from the drug carrier in the form of ZIF-L alone was very low, which is in line with previous studies that used ZIFs in DOX loading and release studies [43,44]. However, the use of ZIF-L as the main framework can strengthen and stabilize the structure so that it does not easily collapse when delivering drugs. In terms of Korsmeyer-Peppas parameters, the n_{KP} of 0.2603 also indicates the diffusion-controlled release mechanism following the Fickian diffusion model [42]. Meanwhile, the k_{KP} value exhibits the structural stability of CNCs/ZIF-L(5) composite where its value (29.2642 h^{-n}) is sufficient to be declared capable of preserving the composite framework from destruction compared to previous studies having lower k_{KP} values. Table 2.

Table 2
Kinetics modelling parameters of DOX release from DOX@CNCs/ZIF-L drug.

Models	Parameters	Values
Higuchi, $f = k_H\sqrt{t}$	k_H – Higuchi constant (hours $^{-0.5}$)	12.7388
	R^2	0.5821
Korsmeyer-Peppas, $f = k_{KP}t^{n_{KP}}$	k_{KP} – structural incorporation constant (hours $^{-n}$)	29.2642
	n_{KP} – drug release mechanism constant (–)	0.2603
	R^2	0.9199

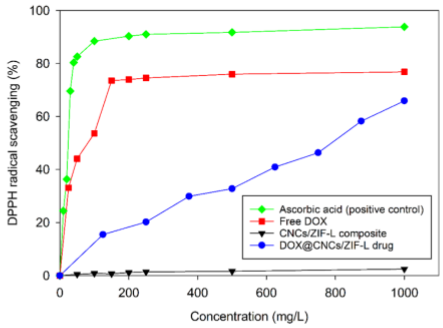

Fig. 6. DPPH radical scavenging profiles of free DOX, CNCs/ZIF-L composite, and DOX@CNCs/ZIF-L drug.

3.4. Antioxidant activity

As an initial effectiveness test, antioxidant activity was performed using the DPPH assay to determine the ability to inhibit free radicals [45]. Fig. 6 shows the DPPH radical scavenging profiles of free DOX, CNCs/ZIF-L(5) composite, and DOX@CNCs/ZIF-L drug. Here, ascorbic acid (positive control) and free DOX showed direct and excellent inhibitory ability even at low concentrations which are also expressed in terms of IC_{50} up to 20.10 and 80.96 mg/L, respectively. This can happen because drug molecules immediately spread in the system and interact directly with free radicals. However, this direct drug delivery system is to be avoided to minimize the side effects that may arise.

Here, the inhibition profile of DOX@CNCs/ZIF-L drug towards free radicals is as expected where the increase in the percentage of inhibition occurs gradually until it reaches >65 % or even higher at high concentrations. Therefore, treatment can be maintained at a certain level that does not pose a risk of side effects. In addition, the IC_{50} value of DOX@CNCs/ZIF-L drug (480.21 mg/L) is higher than free DOX because

Table 3
IC_{50} values of free DOX, CNCs/ZIF-L composite, and DOX@CNCs/ZIF-L drug.

Materials	IC_{50} (mg/L)	IC_{50} in terms of DOX concentration (mg/L)
Ascorbic acid (positive control)	20.10	–
Free DOX	80.96	80.96
CNCs/ZIF-L composite	~	~
DOX@CNCs/ZIF-L drug	788.62	480.21

DOX needs to go through a release mechanism from the CNC/ZIF-L composite first to be able to contact and inhibit free radicals. Here the release mechanism becomes a resistance that must be considered especially in determining drug dosage. However, the IC_{50} value of 480.21 mg/L is satisfactory compared to previous studies where DOX are carried with ZIF-8 and γ-cyclodextrin-MOFs having IC_{50} values of up to 1114.6 and 1000 mg/L, respectively [28,46]. In this study, the CNCs/ZIF-L composite proves to act very well as a drug carrier in terms of loading capacity and release ability while also showing high potential to maintain the effectiveness of DOX in free radical inhibition. Table 3

4. Conclusion

This study has successfully fabricated CNCs/ZIF-L composite through the in-situ method using a green water-based solvent at room temperature. Here, the CNCs addition of 5 % into the fabrication process provides the best composite characteristics with a DOX loading capacity of up to 1508.91 ± 7.72 mg/g. The ability of the CNCs/ZIF-L composite to load DOX is awe-inspiring through a physicochemical mechanism with the formation of multilayer DOX on the composite surface. In addition, DOX (up to 80 % in 1 hour) can be delivered well with a diffusion-controlled release mechanism while maintaining the effectiveness of DOX's free radical scavenging capabilities (IC_{50} = 480.21 mg/L). The great potential shown by the CNCs/ZIF-L composite can continue to be developed and studied in the future to become a commercial drug carrier that is suitable for use in medical applications, especially in the development of chemotherapy.

CRediT authorship contribution statement

Christian J. Wijaya: Writing – review & editing, Writing – original draft, Validation, Resources, Project administration, Methodology, Investigation, Funding acquisition, Data curation, Conceptualization. **Sandy B. Hartono:** Resources, Investigation, Funding acquisition, Data curation, Conceptualization. **Jindrayani N. Putro:** Conceptualization, Data curation, Funding acquisition, Investigation, Resources. **Juliana Anggono:** Funding acquisition, Investigation, Conceptualization, Data curation, Resources. **Tarzan Sembiring:** Validation, Data curation, Conceptualization, Funding acquisition, Investigation, Resources. **Herlian E. Putra:** Validation, Formal analysis, Data curation. **Maria Yuliana:** Investigation, Data curation, Conceptualization, Validation. **Jenni Lie:** Visualization, Validation, Methodology. **Shella P. Santoso:** Visualization, Validation, Methodology. **Chien-Yen Chen:** Validation, Methodology, Formal analysis, Data curation, Conceptualization. **Felycia E. Soetaredjo:** Writing – review & editing, Validation, Methodology, Conceptualization. **Suryadi Ismadji:** Writing – review & editing, Validation, Methodology, Conceptualization. **Setiyo Gunawan:** Writing – review & editing, Validation, Methodology, Conceptualization.

Declaration of competing interest

The authors declare the following financial interests/personal relationships which may be considered as potential competing interests: Christian J. Wijaya reports financial support was provided by the National Research and Innovation Agency of the Republic of Indonesia. If there are other authors, they declare that they have no known competing financial interests or personal relationships that could have appeared to influence the work reported in this paper.

Acknowledgements

The authors would like to thank the National Research and Innovation Agency of the Republic of Indonesia [Grant No. 139/IV/KS/11/2023 or 7041/WM01/H/2023] for the financial support in this research.

References

[1] Velusamy P, Srinivasa CM, Kumar GV, Qurishi Y, Su C-H, Gopinath SCB. A pH stimuli thiol modified mesoporous silica nanoparticles: doxorubicin carrier for cancer therapy. J Taiwan Inst Chem Eng 2018;87:264–71. https://doi.org/10.1016/j.jtice.2018.03.048.

[2] Wan Y, Wang J, Xu J, Tang F, Chen L, Tan Y, et al. Panax ginseng and its ginsenosides: potential candidates for the prevention and treatment of chemotherapy-induced side effects. J Ginseng Res 2021;45:617–30. https://doi.org/10.1016/j.jgr.2021.03.001.

[3] El-Bindary M, El-Bindary A. Synthesis, characterization, DNA binding, and biological action of dimedone arylhydrazone chelates. Appl Organomet Chem 2022;36. https://doi.org/10.1002/aoc.6576.

[4] El-Bindary AA, Toson EA, Shoueir KR, Aljohani HA, MM Abo-Ser. Metal–organic frameworks as efficient materials for drug delivery: synthesis, characterization, antioxidant, anticancer, antibacterial and molecular docking investigation. Appl Organomet Chem 2020;34. https://doi.org/10.1002/aoc.5905.

[5] El-Bindary MA, El-Desouky MG, El-Bindary AA. Metal–organic frameworks encapsulated with an anticancer compound as drug delivery system: synthesis, characterization, antioxidant, anticancer, antibacterial, and molecular docking investigation. Appl Organomet Chem 2022;36. https://doi.org/10.1002/aoc.6660.

[6] Patial S, Sonu Thakur S, Van Le Q, Ahamad T, Singh P, et al. Facile synthesis of Co, Fe-bimetallic MIL-88A/microcrystalline cellulose composites for efficient adsorptive and photo-Fenton degradation of RhB dye. J Taiwan Inst Chem Eng 2023;153:105189. https://doi.org/10.1016/j.jtice.2023.105189.

[7] Mo Z, Zhang H, Shahab A, khan FA, Chen J, Huang C. Functionalized metal-organic framework UIO-66 nanocomposites with ultra-high stability for efficient adsorption of heavy metals: kinetics, thermodynamics, and isothermal adsorption. J Taiwan Inst Chem Eng 2023;146:104778. https://doi.org/10.1016/j.jtice.2023.104778.

[8] Alsuhaibani AM, Alayyafi AAA, Albedair LA, El-Desouky MG, El-Bindary AA. Efficient fabrication of a composite sponge for Cr(VI) removal via citric acid cross-linking of metal-organic framework and chitosan: adsorption isotherm, kinetic studies, and optimization using Box-Behnken design. Mater Today Sustain 2024;26. https://doi.org/10.1016/j.mtsust.2024.100732.

[9] Ahmad I, Muhmood T, Rehman A, Zahid M, Abohashrh M, Nishat S, et al. Zeolite imidazole framework entrapped quantum dots (QDs@ZIF-8): encapsulation, properties, and applications. J Taiwan Inst Chem Eng 2023;149. https://doi.org/10.1016/j.jtice.2023.104993.

[10] Lei C, Gao J, Ren W, Xie Y, Abdalkarim SYH, Wang S, et al. Fabrication of metal-organic frameworks@cellulose aerogels composite materials for removal of heavy metal ions in water. Carbohydr Polym 2019;205:35–41. https://doi.org/10.1016/j.carbpol.2018.10.029.

[11] Ma X, Lou Y, Chen X-B, Shi Z, Xu Y. Multifunctional flexible composite aerogels constructed through in-situ growth of metal-organic framework nanoparticles on bacterial cellulose. Chem Eng J 2019;356:227–35. https://doi.org/10.1016/j.cej.2018.09.034.

[12] Lakshmi BA, Kim S. Current and emerging applications of nanostructured metal–organic frameworks in cancer-targeted theranostics. Mater Sci Eng C 2019;105:110091. https://doi.org/10.1016/j.msec.2019.110091.

[13] Zhou S, Kong X, Zheng B, Huo F, Strømme M, Xu C. Cellulose nanofiber @ Conductive metal-organic frameworks for high-performance flexible supercapacitors. ACS Nano 2019;13:9578–86. https://doi.org/10.1021/acsnano.9b04670.

[14] Cheng L, Yan P, Yang X, Zou H, Yang H, Liang H. High conductivity, percolation behavior and dielectric relaxation of hybrid ZIF-8/CNT composites. J Alloys Compd 2020;825. https://doi.org/10.1016/j.jallcom.2020.154132.

[15] Abdel-Magied AF, Abdelhamid HN, Ashour RM, Zou X, Forsberg K. Hierarchical porous zeolitic imidazolate frameworks nanoparticles for efficient adsorption of rare-earth elements. Microporous Mesoporous Mater 2019;278:175–84. https://doi.org/10.1016/j.micromeso.2018.11.022.

[16] Sevimli-Yurttas Z, Moreira RG, Castell-Perez E. Aggregation and sedimentation stability of nanoscale Zeolitic Imidazolate Framework (ZIF-8) nanocomposites for antimicrobial agent delivery applications. Nano Select 2024. https://doi.org/10.1002/nano.202400029.

[17] Wijaya CJ, Soetaredjo FE, Ismadji S, Gunawan S. Synthesis of cellulose nanocrystals/HKUST-1 composites and their applications: crystal violet removal and doxorubicin loading. Polymers (Basel) 2022;14. https://doi.org/10.3390/polym14224991.

[18] MM Abo-ser, Toson ESA, El-Bindary AA, Schlatter G, Shoueir KR. Smart chitosan nanogel for targeted doxorubicin delivery, ensuring precise release, and minimizing side effects in Ehrlich ascites carcinoma-bearing mice. Int J Biol Macromol 2024;267. https://doi.org/10.1016/j.ijbiomac.2024.131390.

[19] El-Metwaly NM, Katouah HA, El-Desouky MG, El-Bindary AA, El-Bindary MA. Fabricating of Fe3O4@Ag-MOF nanocomposite and evaluating its adsorption activity for removal of doxorubicin. J Environ Sci Health Part A 2022;57:1099–115. https://doi.org/10.1080/10934529.2022.2156230.

[20] Kamelnia E, Divsalar A, Darroudi M, Yaghmaei P, Sadri K. Production of new cellulose nanocrystals from Ferula gummosa and their use in medical applications via investigation of their biodistribution. Ind Crops Prod 2019;139:111538. https://doi.org/10.1016/j.indcrop.2019.111538.

[21] Xiao Y, Liu Y, Wang X, Li M, Lei H, Xu H. Cellulose nanocrystals prepared from wheat bran: characterization and cytotoxicity assessment. Int J Biol Macromol 2019;140:225–33. https://doi.org/10.1016/j.ijbiomac.2019.08.160.

[22] Wijaya CJ, Saputra SN, Soetaredjo FE, Putro JN, Lin CX, Kurniawan A, et al. Cellulose nanocrystals from passion fruit peels waste as antibiotic drug carrier.

Carbohydr Polym 2017;175:370–6. https://doi.org/10.1016/j.carbpol.2017.08.004.
[23] Wijaya CJ, Ismadji S, Aparamarta HW, Gunawan S. Optimization of cellulose nanocrystals from bamboo shoots using Response Surface Methodology. Heliyon 2019;5:e02807. https://doi.org/10.1016/j.heliyon.2019.e02807.
[24] Putro JN, Soetaredjo FE, Irawaty W, Hartono SB, Santoso SP, Lie J, et al. Cellulose nanocrystals (CNCs) and its modified form from durian rind as dexamethasone carrier. Polymers (Basel) 2022;14. https://doi.org/10.3390/polym14235197.
[25] Wijaya CJ, Ismadji S, Aparamarta HW, Gunawan S. Facile and green synthesis of starfruit-like ZIF-L, and its optimization study. Molecules 2021;26:4416.
[26] Anggraini SA, Prasetija KA, Yuliana M, Wijaya CJ, Bundjaja V, Angkawijaya AE, et al. pH-responsive hollow core zeolitic-imidazolate framework-8 as an effective drug carrier of 5-fluorouracil. Mater Today Chem 2023;27. https://doi.org/10.1016/j.mtchem.2022.101277.
[27] AbouAitah K, Higazy IM, Swiderska-Sroda A, Abdelhameed RM, Gierlotka S, Mohamed TA, et al. Anti-inflammatory and antioxidant effects of nanoformulations composed of metal-organic frameworks delivering rutin and/or piperine natural agents. Drug Deliv 2021;28:1478–95. https://doi.org/10.1080/10717544.2021.1949073.
[28] El-Bindary AA, Toson EA, Shoueir KR, Aljohani HA, Abo-Ser MM. Metal–organic frameworks as efficient materials for drug delivery: synthesis, characterization, antioxidant, anticancer, antibacterial and molecular docking investigation. Appl Organomet Chem 2020;34:1–15. https://doi.org/10.1002/aoc.5905.
[29] Ding B, Wang X, Xu Y, Feng S, Ding Y, Pan Y, et al. Hydrothermal preparation of hierarchical ZIF-L nanostructures for enhanced CO2 capture. J Colloid Interface Sci 2018;519:38–43. https://doi.org/10.1016/j.jcis.2018.02.047.
[30] Jian M, Liu B, Liu R, Qu J, Wang H, Zhang X. Water-based synthesis of zeolitic imidazolate framework-8 with high morphology level at room temperature. RSC Adv 2015;5:48433–41. https://doi.org/10.1039/c5ra04033g.
[31] Khan IU, Othman MHD, Ismail AF, Ismail N, Jaafar J, Hashim H, et al. Structural transition from two-dimensional ZIF-L to three-dimensional ZIF-8 nanoparticles in aqueous room temperature synthesis with improved CO2 adsorption. Mater Charact 2018;136:407–16. https://doi.org/10.1016/j.matchar.2018.01.003.
[32] Mahmoodi NM, Keshavarzi S, Oveisi M, Rahimi S, Hayati B. Metal-organic framework (ZIF-8)/inorganic nanofiber (Fe2O3) nanocomposite: green synthesis and photocatalytic degradation using LED irradiation. J Mol Liq 2019;291:111333. https://doi.org/10.1016/j.molliq.2019.111333.
[33] Santoso E, Ediati R, Istiqomah Z, Sulistiono DO, Nugraha RE, Kusumawati Y, et al. Facile synthesis of ZIF-8 nanoparticles using polar acetic acid solvent for enhanced adsorption of methylene blue. Microporous Mesoporous Mater 2021;310:110620. https://doi.org/10.1016/j.micromeso.2020.110620.
[34] Naduparambath S, Jinitha TV, Shaniba V, Sreejith MP, Balan AK. Isolation and characterisation of cellulose nanocrystals from sago seed shells. Carbohydr Polym 2018;180:13–20. https://doi.org/10.1016/j.carbpol.2017.09.088.
[35] Mdlovu NV, Lin K-S, Mavuso FA, Weng M-T. Preparation, characterization, and in-vitro studies of doxorubicin-encapsulated silica coated iron oxide nanocomposites on liver cancer cells. J Taiwan Inst Chem Eng 2020;117:190–7. https://doi.org/10.1016/j.jtice.2020.11.037.
[36] Plazinski W, Dziuba J, Rudzinski W. Modeling of sorption kinetics: the pseudo-second order equation and the sorbate intraparticle diffusivity. Adsorption 2013;19:1055–64. https://doi.org/10.1007/s10450-013-9529-0.
[37] Madaeni SS, Salehi E. Adsorption of cations on nanofiltration membrane: separation mechanism, isotherm confirmation and thermodynamic analysis. Chem Eng J 2009;150:114–21. https://doi.org/10.1016/j.cej.2008.12.005.
[38] Abebe B, Murthy HCA, Amare E. Summary on adsorption and photocatalysis for pollutant remediation: mini review. J Encapsul Adsorpt Sci 2018;08:225–55. https://doi.org/10.4236/jeas.2018.84012.
[39] Kajama MN, Nwogu NC, Gobina E. Hydrogen permeation using nanostructured silica membranes. In: Sustainable development and planning VII. 1. WIT Press; 2015. p. 447–56. https://doi.org/10.2495/sdp150381.
[40] Gholampour N, Eslamian M. Ultrasound-assisted synthesis of layered zeolitic imidazolate framework: crystal formation and characteristics. J Coord Chem 2020;73:317–32. https://doi.org/10.1080/00958972.2020.1713316.
[41] Alasvand N, Urbanska AM, Rahmati M, Saeidifar M, Gungor-Ozkerim PS, Sefat F, et al. Therapeutic nanoparticles for targeted delivery of anticancer drugs. In: Multifunctional systems for combined delivery, biosensing and diagnostics. Elsevier; 2017. p. 245–59. https://doi.org/10.1016/B978-0-323-52725-5.00013-7.
[42] Supramaniam J, Adnan R, Kaus NHM, Bushra R. Magnetic nanocellulose alginate hydrogel beads as potential drug delivery system. Int J Biol Macromol 2018;118:640–8. https://doi.org/10.1016/j.ijbiomac.2018.06.043.
[43] Yan J, Liu C, Wu Q, Zhou J, Xu X, Zhang L, et al. Mineralization of pH-sensitive doxorubicin prodrug in ZIF-8 to enable targeted delivery to solid tumors. Anal Chem 2020;92:11453–61. https://doi.org/10.1021/acs.analchem.0c02599.
[44] Vasconcelos IB, Da Silva TG, Militão GCG, Soares TA, Rodrigues NM, Rodrigues MO, et al. Cytotoxicity and slow release of the anti-cancer drug doxorubicin from ZIF-8. RSC Adv 2012;2:9437–42. https://doi.org/10.1039/c2ra21087h.
[45] Khalil I, Yehye WA, Etxeberria AE, Alhadi AA, Dezfooli SM, Julkapli NBM, et al. Nanoantioxidants: recent trends in antioxidant delivery applications. Antioxidants 2020;9. https://doi.org/10.3390/antiox9010024.
[46] Ke F, Zhang M, Qin N, Zhao G, Chu J, Wan X. Synergistic antioxidant activity and anticancer effect of green tea catechin stabilized on nanoscale cyclodextrin-based metal–organic frameworks. J Mater Sci 2019;54:10420–9. https://doi.org/10.1007/s10853-019-03604-7.

Cellulose nanocrystals/zeolitic imidazolate framework-L(CNCs/ZIF-L) composites for loading and diffusion-controlled release of doxorubicin hydrochloride

ORIGINALITY REPORT

3%	3%	4%	1%
SIMILARITY INDEX	INTERNET SOURCES	PUBLICATIONS	STUDENT PAPERS

PRIMARY SOURCES

1	Christian J. Wijaya, Suryadi Ismadji, Hakun W. Aparamarta, Setiyo Gunawan. "Facile and Green Synthesis of Starfruit-Like ZIF-L, and Its Optimization Study", Molecules, 2021 Publication	1%
2	Christian J. Wijaya, Stephanie N. Saputra, Felycia E. Soetaredjo, Jindrayani N. Putro et al. "Cellulose nanocrystals from passion fruit peels waste as antibiotic drug carrier", Carbohydrate Polymers, 2017 Publication	1%
3	tjnpr.org Internet Source	1%
4	Sreejith Govindan, Rudra Nath Ghosh, Chaithra, Vaidehi Basavakumar Roopa et al. "Evaluation of the Antimicrobial and Organic Dye Removal Properties of Silver-Incorporated ZIF-L Metal–Organic Framework Nanoparticles", ACS Omega, 2025 Publication	1%

Exclude quotes	On	Exclude matches	< 1%
Exclude bibliography	On		

Cellulose nanocrystals/zeolitic imidazolate framework-L(CNCs/ZIF-L) composites for loading and diffusion-controlled release of doxorubicin hydrochloride

GRADEMARK REPORT

FINAL GRADE

/100

GENERAL COMMENTS

PAGE 1

PAGE 2

PAGE 3

PAGE 4

PAGE 5

PAGE 6

PAGE 7

PAGE 8